FINAL REPORT

"Fiber-Optic Sensor with Simultaneous Temperature, Pressure, and Chemical Sensing Capabilities"

DOE Award No.: DE-FG02-05ER86262

Recipient: MicroMaterials, Inc.
13302 Telecom Dr.
Tampa, Fl 33637

P.I.: Jermaine L. Kennedy, Ph.D.

Partner: University of South Florida

SUMMARY

This project aimed to develop a multifunctional sensor suitable for process control application in chemical and petrochemical industries. Specifically, the objective was to demonstrate a fiber optic sensing system capable of simultaneous temperature, pressure, and chemical composition determinations based on a single strand of sapphire optical fiber. These capabilities were to be achieved through the incorporation of a phosphor and a Bragg grating into the fiber, as well as the exploitation of the evanescent field interaction of the optical radiation inside the fiber with the surrounding chemical medium. The integration of the three functions into a single probe, compared to having three separate probes, would not only substantially reduce the cost of the combined system, but would also minimize the intrusion into the reactor. Such a device can potentially increase the energy efficiency in the manufacture of chemical and petrochemical products, as well as reduce waste and lead to improved quality.

In accordance with the proposed research plan, the individual temperature, pressure and chemical sensors where fabricated and characterized first. Then towards the end of the program, an integrated system was implemented. The sapphire fibers were grown on a laser heated pedestal growth system. The temperature sensor was based on the fluorescence decay principle, which exploits the temperature dependence of the fluorescence decay rate of the selected phosphor. For this project, Cr^{3+} was chosen as the phosphor, and it was incorporated into the sapphire fiber by coating a short length of the source rod with a thin layer of Cr_2O_3. After the viability of the technique was established and the growth parameters optimized, the temperature sensor was characterized up to 300 ˚C and its long term stability was verified. The chemical sensor determined the

concentration of chemicals through evanescent field absorption. Techniques to increase the sensitivity of the evanescent field interaction such as tapering and coiling the fiber were successfully demonstrated. It was shown that the sensor is capable of quantitative measurements in both the mid-infrared and the near infrared regions of the spectrum.

For the pressure sensor, a novel concept involving a pressure amplifier was investigated. While the basic idea was found to work, technical difficulties prevented the demonstration of a sensor capable of quantitative pressure measurements. As a result, the final combined probe contained only a temperature sensor and a chemical sensor.

Under this program not only was the technical feasibility of a dual temperature/chemical sensor demonstrated, so were those of two ancillary devices. The first is a scan-and-dwell fiber optic mid-IR spectrometer specifically designed for process control applications. Also, a versatile high-brightness fiber optic light source with interchangeable emitting elements to cover different spectral regions has been demonstrated. The commercial potentials of the complete system as well as the individual components are being actively explored now.

INTRODUCTION

The objective of this program was to develop a sensing system capable of simultaneous temperature, pressure, and chemical composition measurements using a single sapphire optical fiber probe. The fiber was to consist of three sections, each processed and/or optimized for one of the functions. The temperature sensor makes use of a Cr^{3+} doped portion of the fiber, and derives its functionality through the temperature-dependent fluorescence decay rate of $Cr:Al_2O_3$ (ruby) phosphor. The pressure sensor is based on the Bragg reflection from a grating inscribed into another section of the fiber, while chemical sensing is made possible by evanescent field absorption in a coiled section of the fiber with reduced diameter.

The incorporation of Cr into the sapphire fiber by coating a short length of the source rod used in the fiber fabrication process (by laser heated pedestal growth) with a thin layer of Cr_2O_3 was successfully demonstrated for the first time. After optimization of the growth parameters, the ruby temperature sensor was characterized in terms of its accuracy and shown to be stable against repeated thermal cycling up to 300 ˚C. The sensitivity of the evanescent field sensor was found to be significantly better than predicted. As a result, it was shown that one can obtain useful results in the near-IR as well as the mid-IR region of the spectrum. The Bragg grating pressure sensor was based on a novel concept in which a bellows was used as a pressure amplifier. While the basic effect was observed, the results were eratic. Therefore, the final integrated probe contained only the temperature and chemical sensors.

In the following sections the experimental results obtained on the three individual sensors will be described, followed by a description of the integrated probe. An assessment of the commercial potential of the components and devices developed under this program is given at the end.

TEMPERATURE SENSOR

Starting from 1 mm x 1 mm sapphire feeds, source rods ranging in diameter from 300 μm to 500 μm were grown on MMI's laser heated pedestal growth (LHPG) system. These source rods were sent to a vendor to be coated circumferentially with a thin film of Cr_2O_3 measuring 1 – 2 μm in thickness and covering a length of 1 – 2 mm. We found that increasing the thickness of the Cr_2O_3 coating from 1 μm to 1.5 μm led to unstable growth, resulting in a ruby section with poor crystalline quality (as evidenced by strong light scattering) which is often accompanied by a kink in the fiber. Likewise, increasing the growth rate to more then 3 mm/min led to inferior crystallinity of the ruby. Therefore, all temperature probes characterized in this project were grown from source rods with 1 μm thick Cr_2O_3 coatings at 3mm/min.

The response of the temperature sensor was investigated first. A typical fluorescence decay signal near 690 nm is shown in Fig. 1. The semi-logarithmic plot of the same decay trace is shown in Fig. 2. The straightness of the line indicates that the decay is a pure exponential. This was found to be the case for all the temperatures up to 300 ˚C. The variation of the fluorescence lifetime with temperature is shown in Fig. 3. Actually, the composite of three separate runs is shown here. Since the temperature

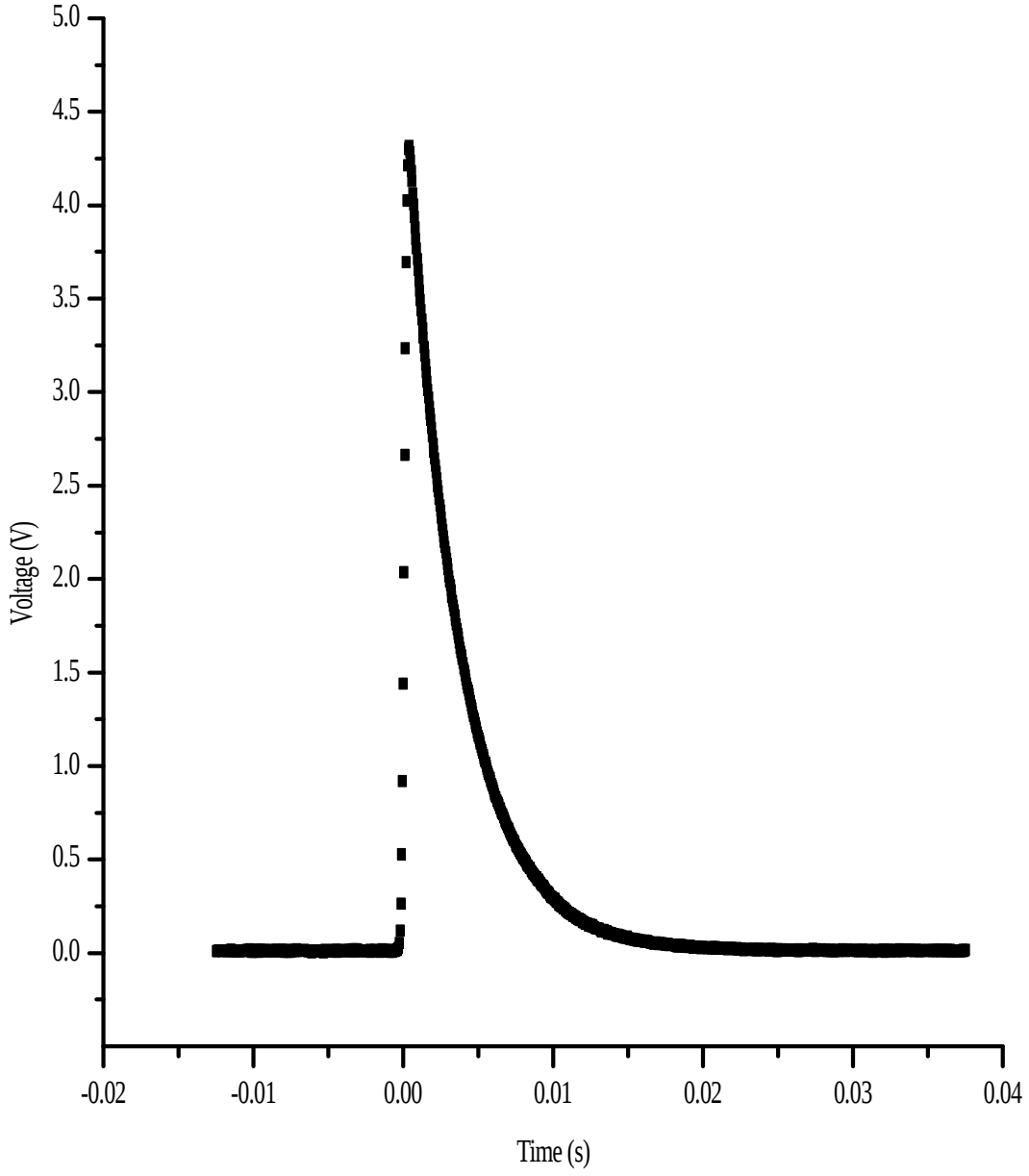
5.0
4.5
4.0
3.5
3.0
2.5
2.0
1.5
1.0
0.5
0.0
Voltage (V)
-0.02
-0.01
0.00
0.01
0.02
0.03
0.04
Time (s)

Fig. 1

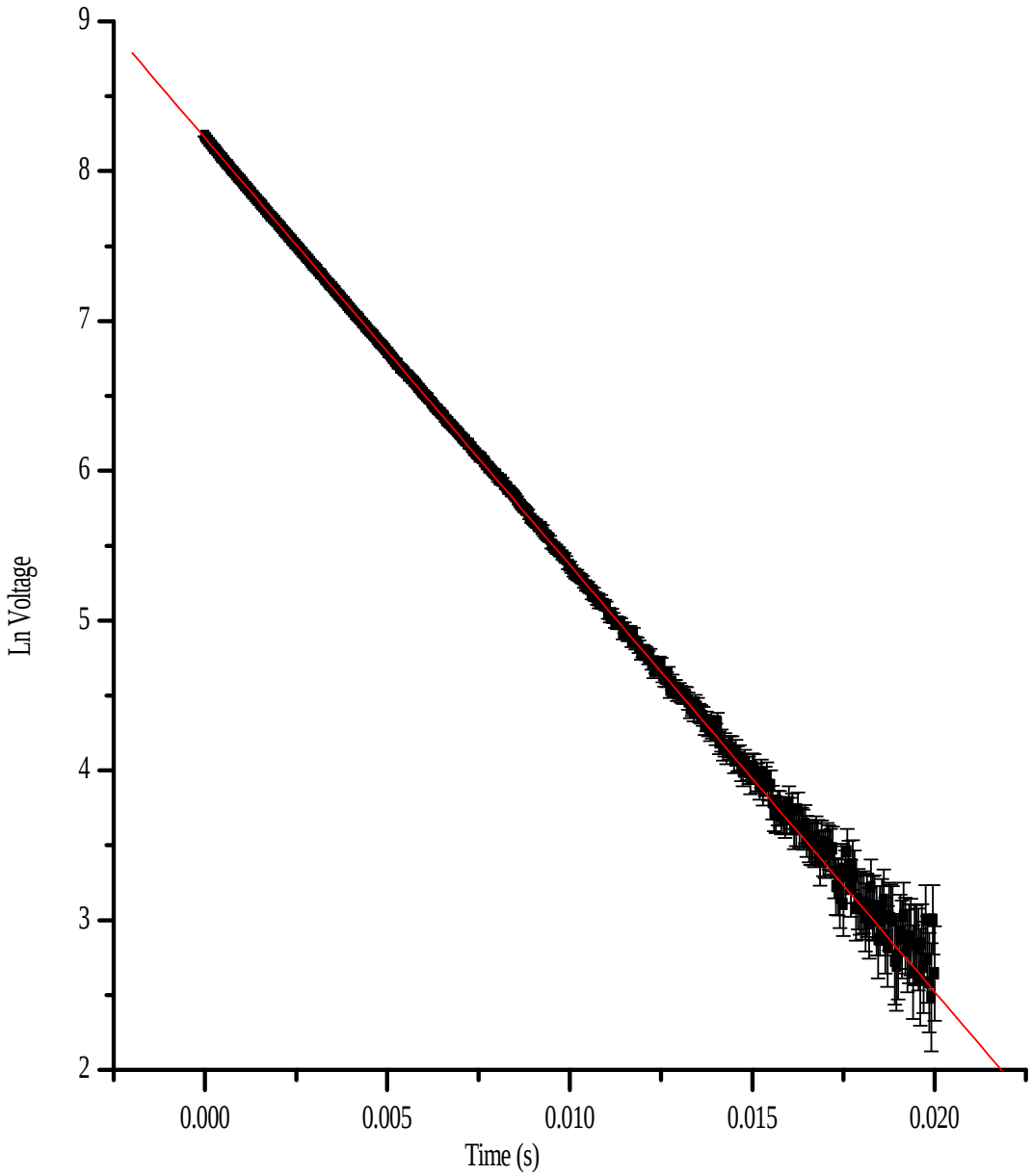

Fig. 2

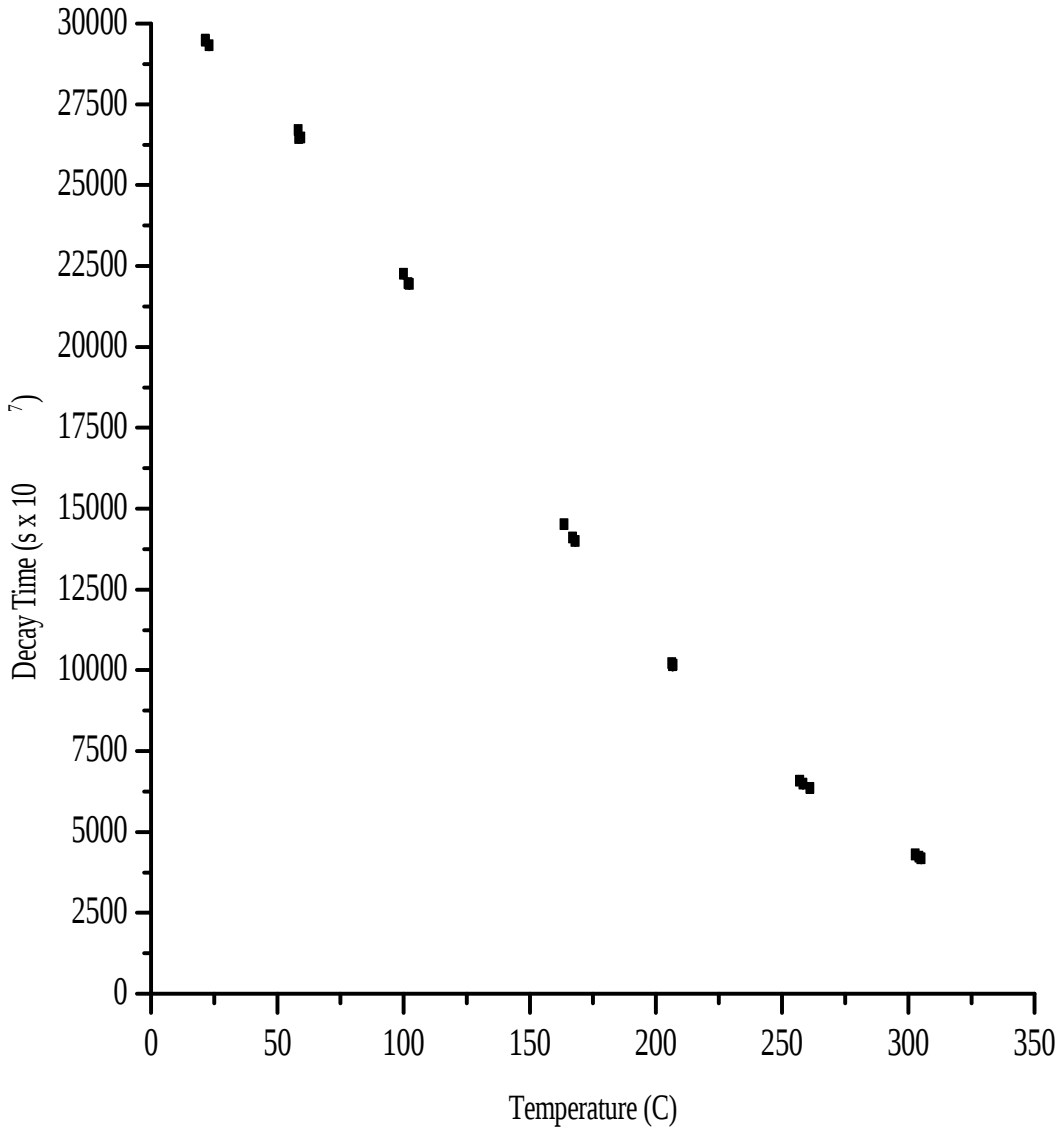
30000
27500
25000
22500
20000
17500
15000
12500
10000
7500
5000
2500
0
Decay Time (s x 10 7)
0
50
100
150
200
250
300
350
Temperature (C)

Fig. 3

cannot be accurately reproduced in each instance, most of the data appear as clusters. In fact, the single point near 200 ˚C represents three points lying on top of each other. In any event, it is evident that the variation of the fluorescence decay time with temperature is highly reproducible over this temperature range. In these measurements the probe was placed in a heated quartz tube, with a thermocouple positioned within 1mm of the Cr doped section of the probe.

The stability of the sensor near the maximum temperature of 300 ˚C was studied next. The results obtained during a 51 hour run are shown in Fig. 4. Over this time period, the temperature inside the heating tube fluctuated approximately +/- 5 ˚C. Each data point represents the average of 5 readings taken over several seconds. The number above each point indicates how many hours has passed since the start of the run. While this figure shows the uncertainty in the fluorescence decay time at a given temperature, one can also conclude that the uncertainty in the temperature measurement for a given measured decay time is no more then +/- 1 ˚C near 300 ˚C.

To find out the axial distribution of Cr^{3+} ions in the doped part of the fiber, spatially resolved side light emission measurements were made. A 200 μm fiber grown from a 300 μm source fiber coated with 1 μm thick Cr_2O_3 over a 2 mm length was used for this purpose. Using a single lens, the emission was imaged onto a detector fitted with a 0.3 mm slit. The measured fluorescence signals as the detector was scanned are shown as filled circles in Fig. 5. It is seen that most of the emission comes from a 2 mm doped section of the fiber, which gives a measure of the spatial resolution of the temperature sensor.

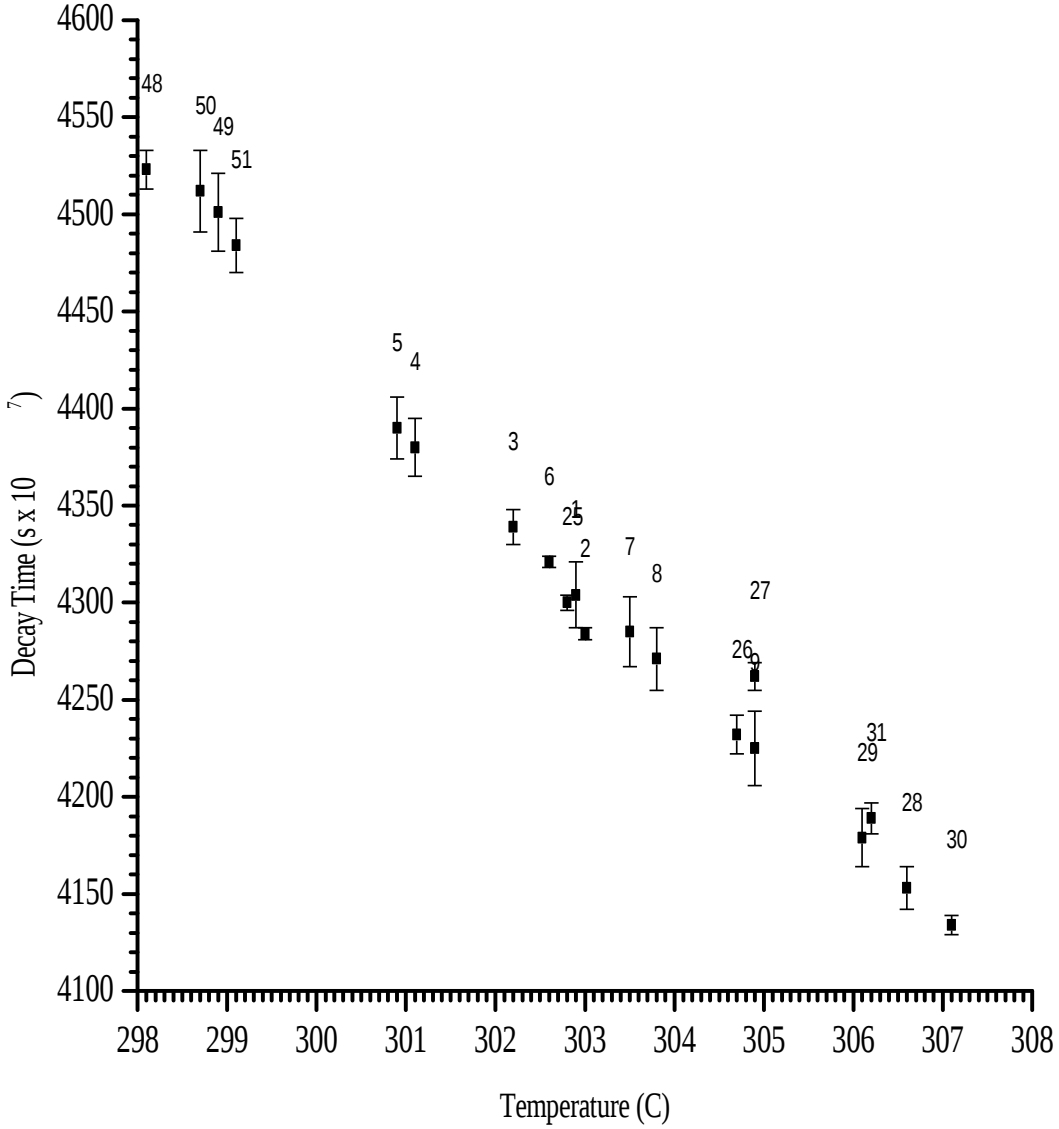
Decay Time (s x 10 7)
Temperature (C)
4600
4550
4500
4450
4400
4350
4300
4250
4200
4150
4100
298
299
300
301
302
303
304
305
306
307
308
48
50
49
51
5
4
3
6
1
25
2
7
8
27
26
9
31
29
28
30

Fig. 4

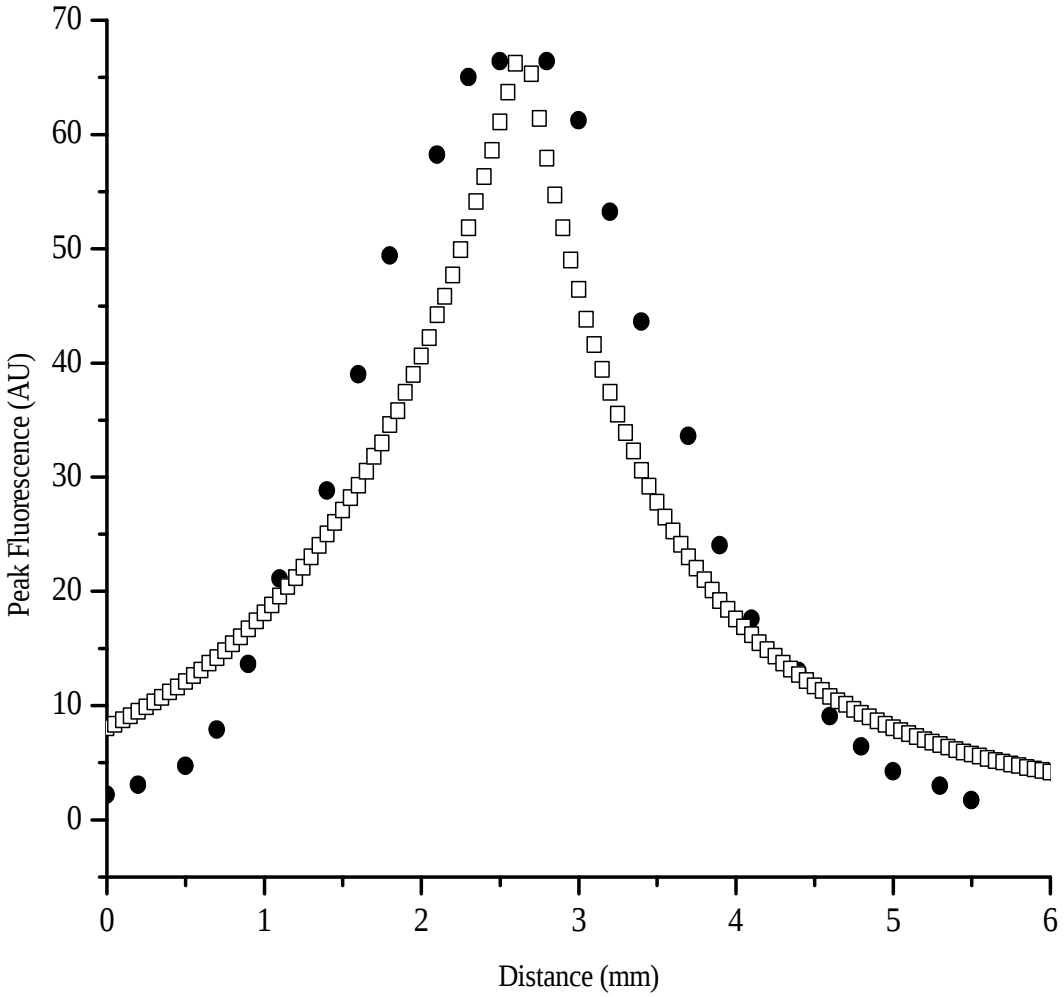
70
60
50
40
30
20
10
0
Peak Fluorescence (AU)
0
1
2
3
4
5
6
Distance (mm)

Fig. 5

To estimate the extent of the Cr loss incurred in the growth process, numerical modeling of the axial emission profile was undertaken. The model takes into account both Cr loss and the fractional distribution coefficient for the incorporation of Cr ions into Al_2O_3. Assuming a uniform concentration of Cr in the molten zone, then, its concentration in the grown fiber is given by

$$C(x) = C_0\,[1-exp(-kx/r^2 l)], \qquad 0 < x < r^2 L \tag{1}$$

$$C(x) = C_0\,[exp(kL/l)-1]\,exp(-kx/r^2 l), \quad x > r^2 L \tag{2}$$

In these equations, k is the distribution coefficient, r the diameter reduction ratio, L the length of the coated portion of the source rod, and l the effective length of the molten zone. Also, $x = 0$ corresponds to the point along the grown fiber when Cr incorporation begins, and C_0 is the Cr concentration in the molten zone at $x = 0$ after loss due to evaporation has been taken into account. The power of the excitation light source is given by

$$P(x) = P_0\,exp(-\int_0^x \alpha(x)dx) \tag{3}$$

where P_0 is the power launched into the fiber and $\alpha(x)$ is the absorption coefficient due to Cr^{3+} at the excitation wavelength. For 532 nm light $\alpha(x) = 3{,}500\ C(x)\ cm^{-1}$. Finally, the relative fluorescence intensity can be found from

$$I(x) \sim P(x)C(x) \tag{4}$$

Using the parameters $r = 1.5$, $k = 0.2$, $L = 2$ mm, and $l = 0.2$ mm, the relative axial emission intensity was calculated and the results are shown in Fig. 5 as open circles after normalization to the peak of the measured axial emission profile. The measured peak is broader because of the relatively wide slit used and probably also because of some distortion at the surface of the roughly hexagonal fiber. We speculate that the broad

wings of the calculated profile may be an indication that Cr loss in the molten zone is more pronounced when its concentration is low.

From Eqs. (1) and (2) it is evident that the Cr concentration reaches a maximum value, C_m, when $x = r^2L$. With the parameters given earlier, one finds that $C_m = 0.87C_0$. The Cr concentration in the grown fiber never quite reaches that in the already depleted molten zone (at $x = 0$) because of the small distribution coefficient. One can also determine C_0 from the measured transmission of the 532 nm excitation laser beam by using Eq. (3), and it is found to be 0.25 %. If there were no Cr loss, and assuming the Cr_2O_3 to be 100 % dense, one finds that the expected Cr density would be 1.2 %. Thus, approximately 30 % of the Cr is lost through evaporation in the laser heated pedestal growth process.

We have also investigated the dependence of fluorescence decay time on Cr^{3+} concentration. The 532 nm laser beam was focused to a line with the use of a cylindrical lens in order to excite the phosphor from the side of the fiber with high spatial resolution. The fluorescence guided to one end of the fiber was then detected. We found that the decay time at room temperature from the point corresponding to the maximum Cr^{3+} concentration was approximately 2 % lower than those from the far wings of the doped region. Thus, the actual decay time measured by the temperature sensor represents an average, albeit the range of values being averaged is a small one.

The effect of the refractive index of the fluid in which the ruby temperature sensor is immersed on fluorescence decay time has also been investigated. A difference of not quite 2 % was found between air and glycerol ($n = 1.47$). This indicates that the large index difference between ruby ($n = 1.73$) and air is causing a small amount of radiation

trapping of the fluorescence. However, the lifetime difference between water (n = 1.33) and glycerol as the immersion medium is only about 0.5 %, essentially the same as the error limits of the measurement. This means that, after the temperature sensor is calibrated in air, a correction must be applied for use in liquids. However, this correction should be valid for essentially all liquids, since few have refractive index smaller than 1.33 or greater than 1.47.

CHEMICAL SENSOR

Chemical sensing through evanescent field absorption in a sapphire optical fiber was motivated by the fact that it is more robust, both chemically and mechanically, than an unclad standard silica fiber. Under this program we have demonstrated that such a sensor is capable of quantitative measurements in both the mid-IR and near-IR regions of the spectrum. In related work, we have also developed a novel fiber optic IR source and a fiber optic near/mid-IR spectrometer which were specifically designed for use with the evanescent field probe. In this section, the performance of these components will be discussed in turn.

The evanescent field sapphire fiber chemical sensor was characterized using the 3 μm band of H_2O first. The fiber used in these experiments had a diameter of 75 μm, with one end tapered up to 150 μm, and a length of 50 cm. Fig. 6 shows the transmitted signals with the fiber in air and approximately 10 cm of a nearly straight section of the fiber immersed in H_2O. Fig. 7 shows the transmitted signals for the same fiber with one section coiled into 2 turns with a radius of 1 cm, again for air and for the helical section

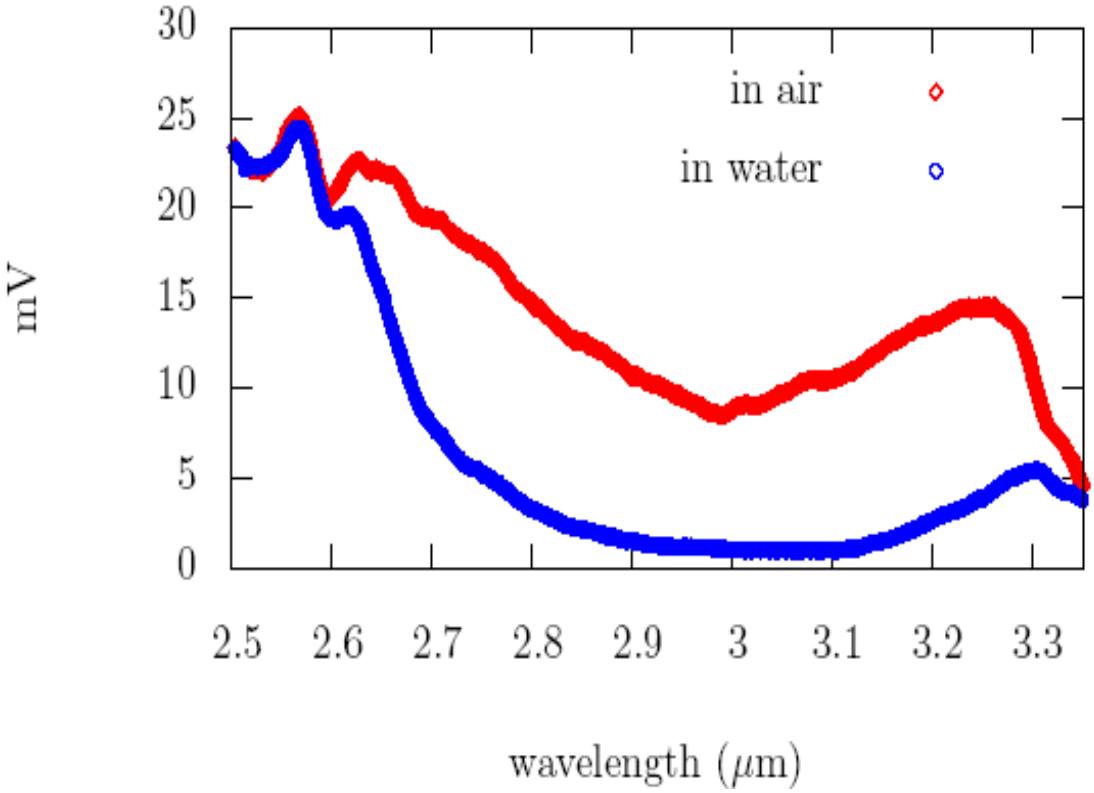
30
25
20
15
10
5
0
mV
in air
in water
2.5
2.6
2.7
2.8
2.9
3
3.1
3.2
3.3
wavelength (μm)

Fig. 6

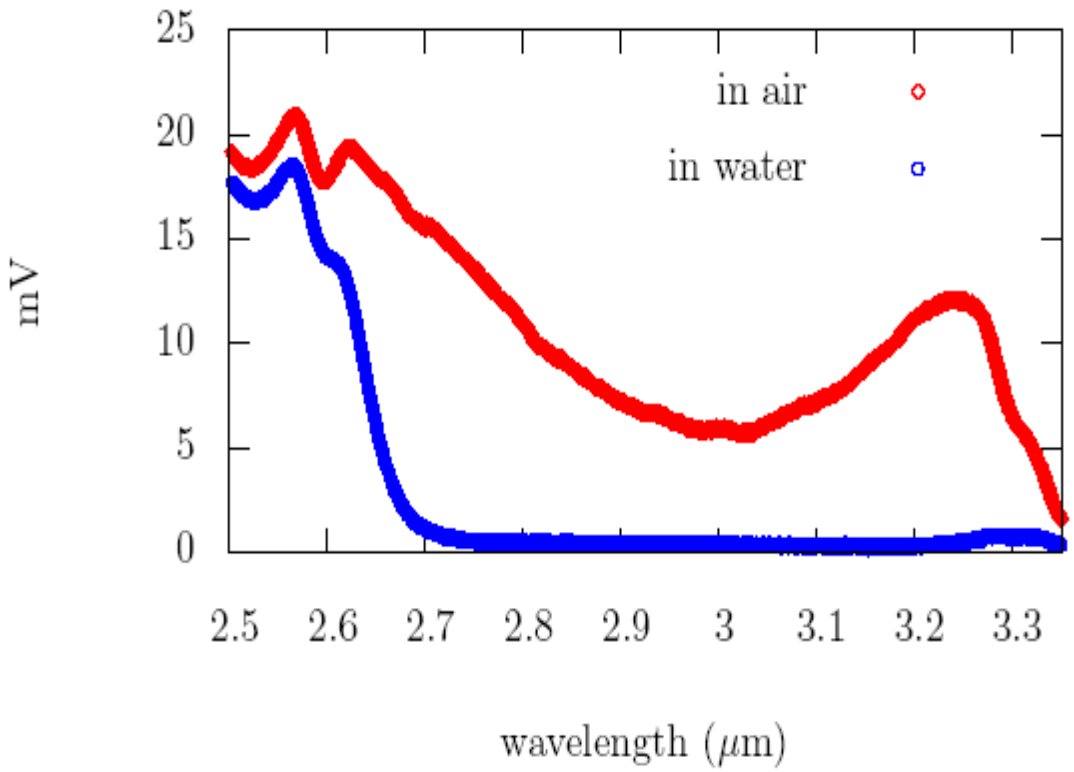
25
20
15
10
5
0
mV
in air
in water
2.5
2.6
2.7
2.8
2.9
3
3.1
3.2
3.3
wavelength (μm)
Fig. 7

in H_2O. It is apparent that coiling the fiber significantly increases the absorption of the evanescent field by the 3 μm band in H_2O. This follows because in a bent fiber a larger percentage of the rays are propagating at angles close to the critical angle for total internal reflection, with their evanescent fields interacting more strongly with the surrounding medium.

To asses the ability of our chemical sensor for trace detection in the mid-IR, we made absorption measurements in D_2O diluted with H_2O. For these studies a 60 μm sapphire fiber was coiled into 8 loops of 0.5 cm radius. The transmitted signals for undiluted D_2O (99.8 % pure according to the vendor and assumed to have 0.2 % H_2O) and the same sample after the addition of 0.7 % H_2O are shown in Fig. 8. Similar data were obtained for additions of 0.2 %, 1.6 %, and 3.2 % H_2O. Fig 9 shows the measured absorption at 2.8 μm vs. H_2O concentration (including the 0.2 % in the undiluted D_2O). The wavelength 2.8 μm instead of the peak wavelength of 2.95 μm was used because signal-to-noise was inadequate at the latter, especially for the higher concentrations. Two observations can be made. First, it appears that the response of the probe is linear up to an integrated absorption as large as 4. Also, since an absorption of 10 % is readily measurable, we see that H_2O concentrations significantly lower than 0.1 % should be detectable on the 3 μm band, especially if the determination is made at the peak wavelength. We were not able to verify this because we did not have confidence in the measurement of H_2O in volumes less than 0.1 ml with the pipette that was available.

The suitability of the chemical sensor in quantifying low concentration species in mixtures by using the much weaker near-IR absorption bands was also investigated. For these studies, small amounts of H_2O were mixed into ethanol (99.5 % pure according to

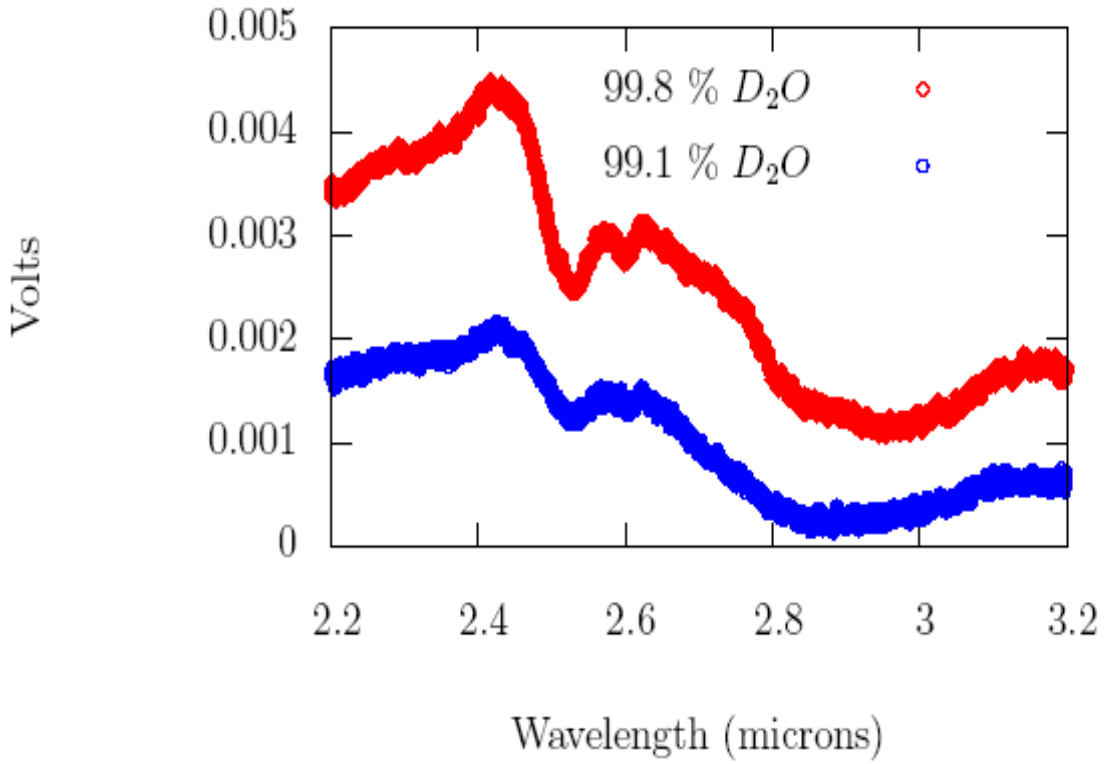
0.005
0.004
0.003
0.002
0.001
0
Volts
99.8 % D_2O
99.1 % D_2O
2.2
2.4
2.6
2.8
3
3.2
Wavelength (microns)

Fig. 8

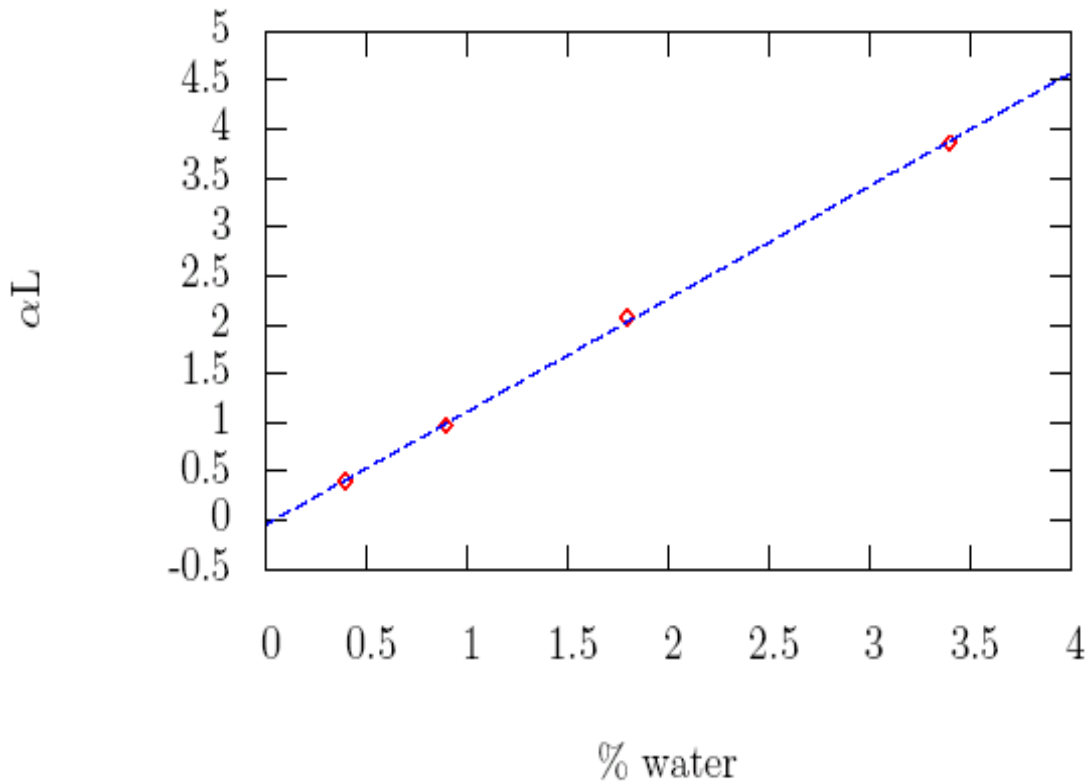

Fig. 9

vendor specification). The 65 μm fiber used was tapered up to 140 μm for the input end, and coiled into 3 loops with a radius of 0.5 cm. The absorption spectra on the 1.9 μm band of H_2O for concentrations up to 10 % are shown in Fig. 10. The areas under the curves between 1.83 μm and 1.98 μm were calculated, and from the results the predicted vs. actual concentration plot shown in Fig. 11 was obtained. It is seen that for the most part the deviation of the spectroscopically determined concentration from the actual prepared concentration is 0.5 % or less. From Fig. 10 it can be seen that at 10 % H_2O the peak absorption corresponds to an αL of 0.25. At higher H_2O concentrations we observed a clear sublinear increase in the value of αL.

That the integrated absorption ceases to grow linearly with H_2O concentration for $\alpha L > 0.2$ near 1.9 μm, whereas it remains linear for αL up to 4 near 3 μm, requires some explanation. This may be due in part to the fact that ethanol has a larger refractive index than D_2O. As a result, the critical angle is larger when ethanol is the solvent. But we believe the main reason is that the fiber used in the near-IR measurements had its imput end tapered to a larger diameter. Therefore, the rays propagating in the fiber on the whole have larger angles. While the very large angle rays increase the sensitivity of the probe, they are more quickly stripped off by the bent fiber. As a result, the net absorption begins to show “saturation” at a relatively low αL value of about 0.2.

The susceptibility of the sapphire fiber to adsorption of the chemical being probed was also investigated. Methylene Blue, a molecule known to exhibit strong adsorption tendency on standard silica fibers, dissolved in water was used in these studies. A flow system incorporating a cuvette was constructed for this purpose. The cuvette was first filled with deionized water in order to establish the baseline transmitted power from a

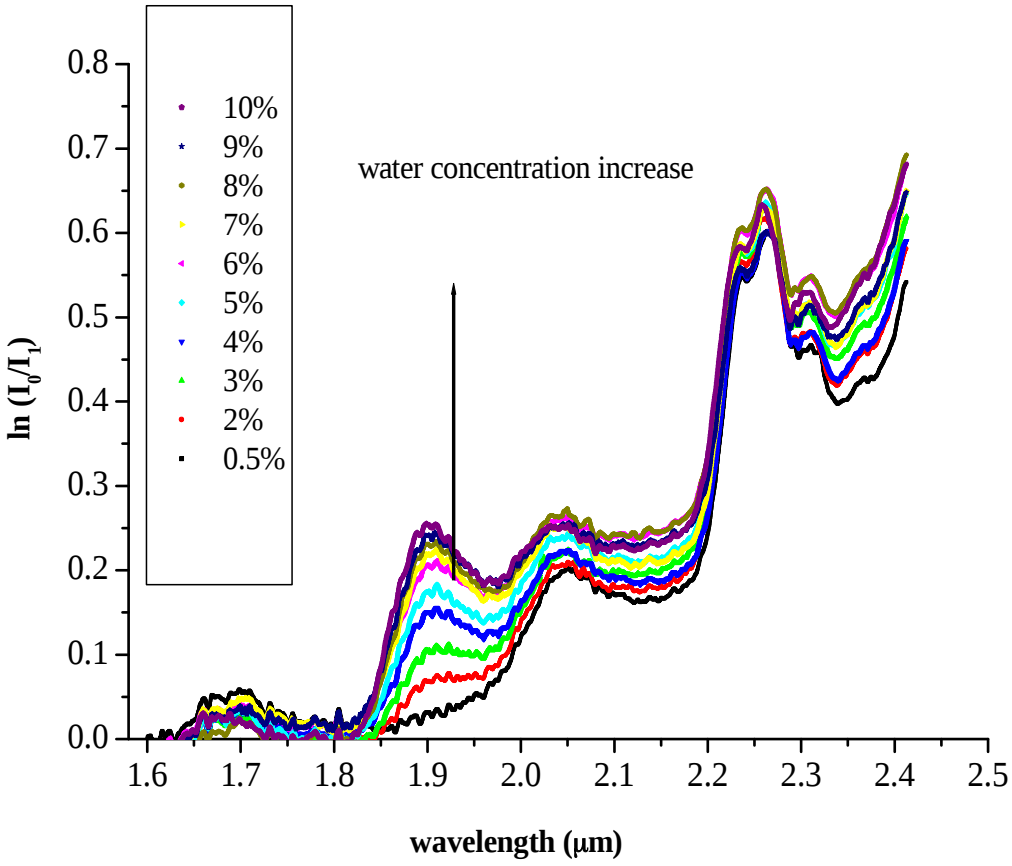
0.8
0.7
0.6
0.5
0.4
0.3
0.2
0.1
0.0
ln (I0/I1)
10%
9%
8%
7%
6%
5%
4%
3%
2%
0.5%
water concentration increase
1.6
1.7
1.8
1.9
2.0
2.1
2.2
2.3
2.4
2.5
wavelength (μm)

Fig. 10

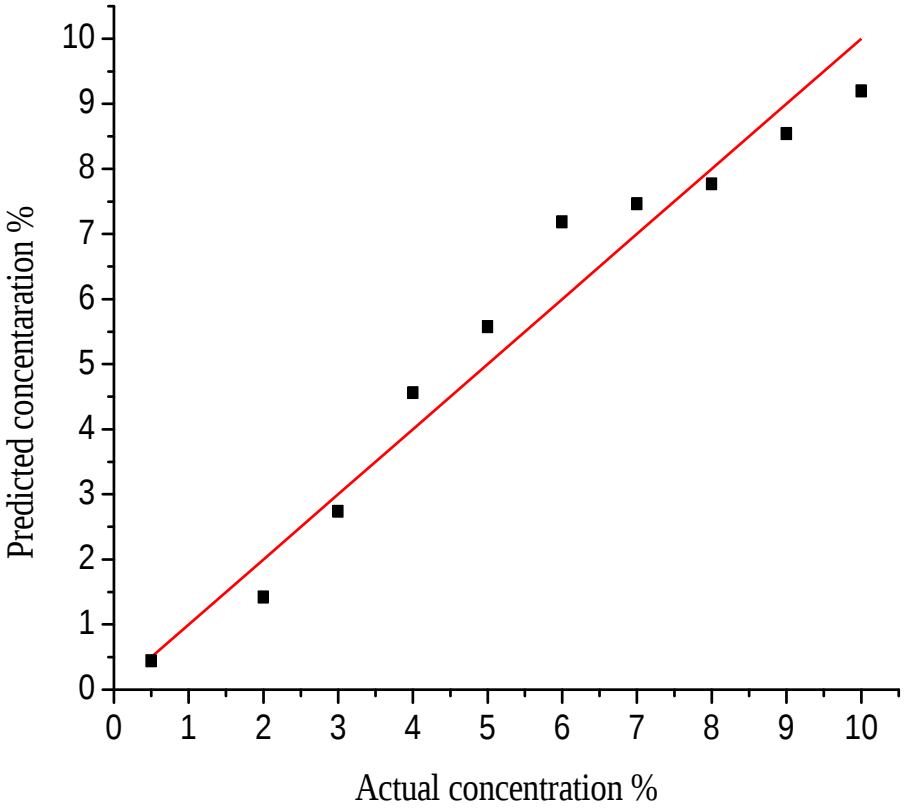
Predicted concentaration %
Actual concentration %
0
1
2
3
4
5
6
7
8
9
10

Fig. 11

stabilized He-Ne laser. A Methylene Blue solution was then introduced into the cuvette to displace the water and produce an evanescent wave absorption at 633 nm of approximately 20 %. Once the transmitted output had stabilized, deionized water was allowed to flow into the cuvette and the recovery of the transmitted output was monitored. It was found that the time required to recover to the initial level was only slightly longer than the time for absorption to equilibrate, indicating that adsorption on the sapphire fiber had a negligible effect. This bodes well for the rapid response of the chemical sensor to changes in the composition of a reactor stream.

In an ancillary effort, we also set out to develop a series of high brightness fiber optic IR light sources. At the heart of these light sources is a laser-powered thermal source consisting of a YAG fiber terminating in a YbAG tip. When 5 W of power from a laser diode was launched into the tip, it was sufficient to melt the YbAG, which has a melting point of approximately 1,900 ˚C. The tip was then coated with various mixtures of emitters in powder form by using a high temperature binder. A photograph of a prototype lightsource is shown in Fig. 12. Thus far, a total of 8 emitter mixtures have been tested. The emission spectrum for one of them is shown in Fig. 13, along with that from a conventional IR source. These spectra have not been corrected for grating or detector response. It is seen that, in some spectral region, the intensity from our light source is as much as three times higher than that of the conventional source. We believe these light sources will be valuable in process control, since only absorption measurements at selected wavelengths are needed in such application.

The spectrometer developed under this program is unique in that, to our knowledge, it is the only fiber-coupled instrument that spans the near IR as well as an

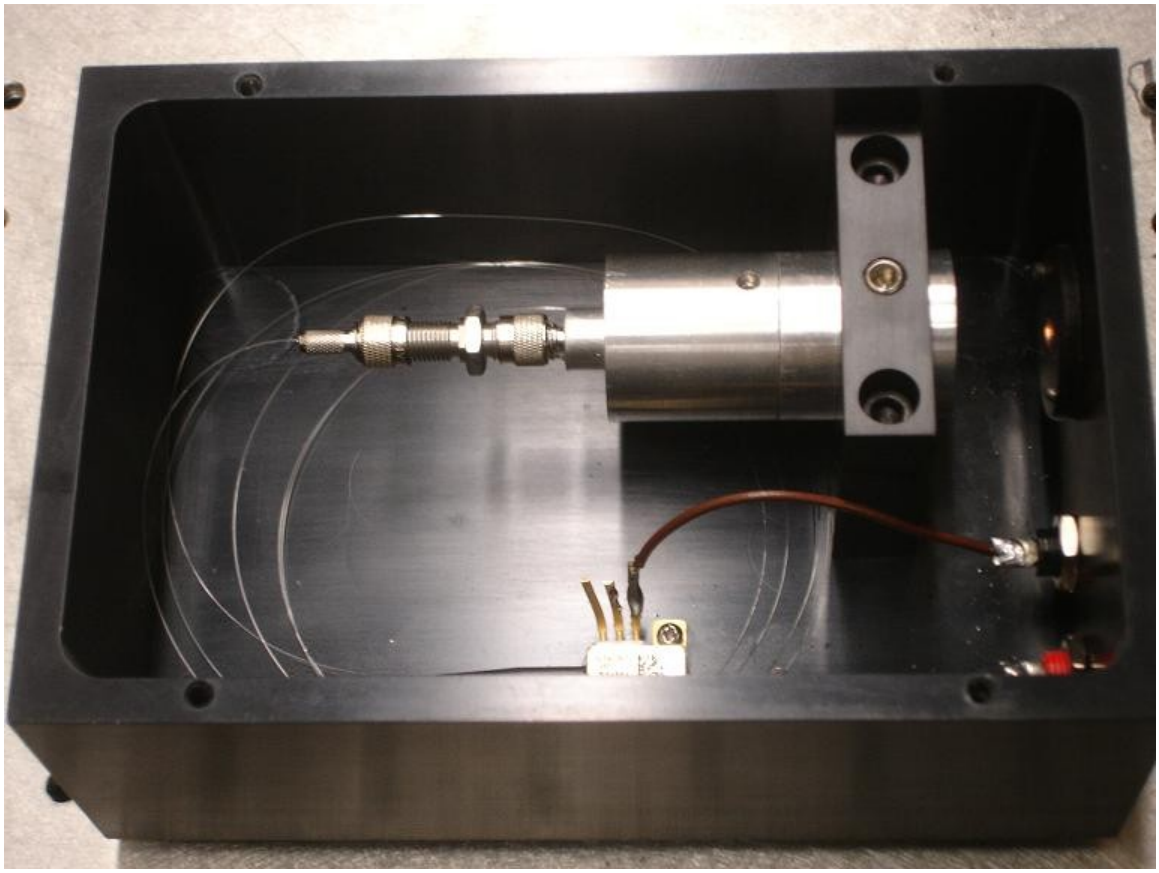

Fig. 12

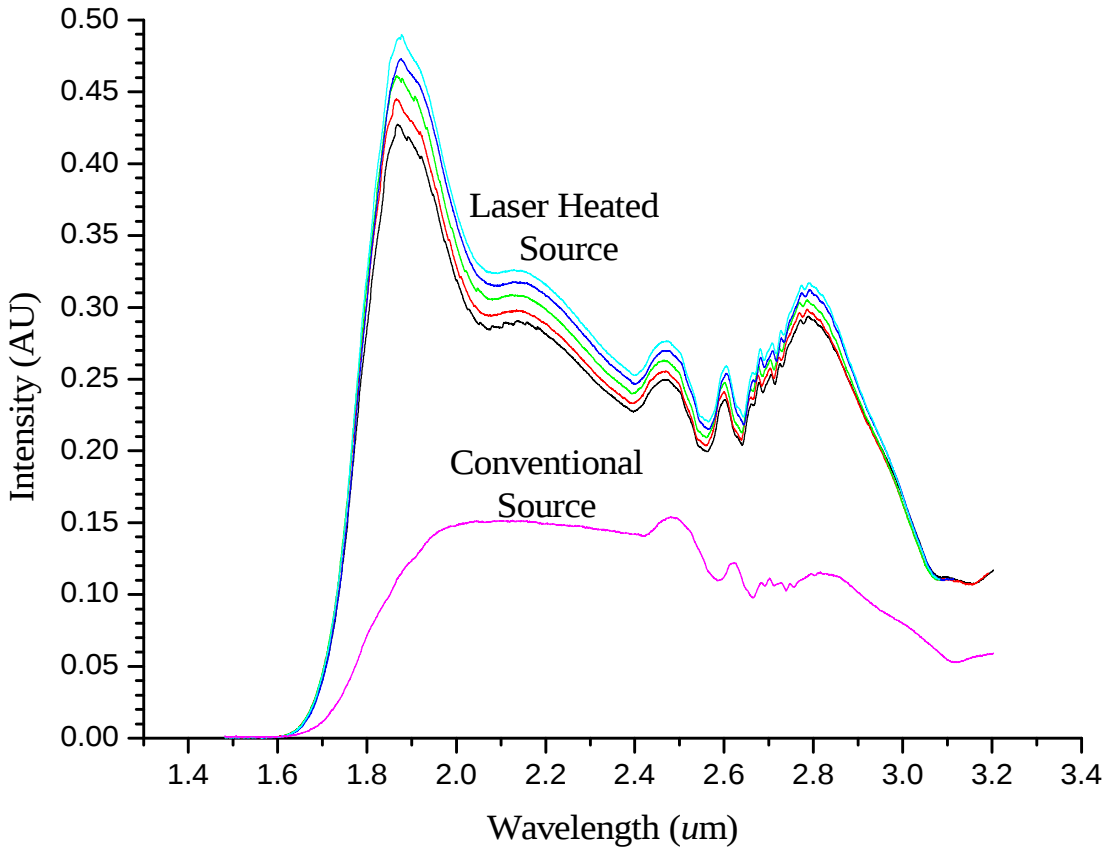
0.50
0.45
0.40
0.35
0.30
0.25
0.20
0.15
0.10
0.05
0.00
Intensity (AU)
Laser Heated
Source
Conventional
Source
1.4
1.6
1.8
2.0
2.2
2.4
2.6
2.8
3.0
3.2
3.4
Wavelength (um)

Fig. 13

important part of the mid-IR. It uses a thermoelectrically cooled InAs detector, and covers the wavelength range from 1 to 3.4 μm. Its scan-and-dwell feature allows rapid scanning through unimportant spectral regions and stopping at selected wavelengths for data acquisition. On-board data processing is accomplished with a powerful microprocessor, and synchronization with external components and light sources is facilitated by a 14-pin digital interface. These features should make it a valuable tool for in-line process control in the chemical industry. A photograph of the interior of the spectrometer is shown in Fig. 14.

PRESSURE SENSOR

The pressure sensor concept is based on a sapphire fiber inscribed with a Bragg grating and sealed into a compressed bellows. Thus, when the external pressure is the same as the ambient pressure at which the sealing is performed, the fiber is in a stretched state, giving a peak interference wavelength for the fiber Bragg grating (FBG) which is longer than that for the unstretched fiber. As the external pressure is increased, the bellows are compressed even more, thereby reducing the tension on the fiber, leading to a decrease in the peak interference wavelength. At a sufficiently high pressure, the tension on the fiber drops to zero. Beyond that, the peak interference wavelength for the FBG will be the same as that for the unstretched fiber. Thus, the bellows acts as a pressure "amplifier," increasing the pressure sensitivity of the FBG by approximately the ratio of the cross-sectional area of the bellows to that of the fiber. The gratings used in our work

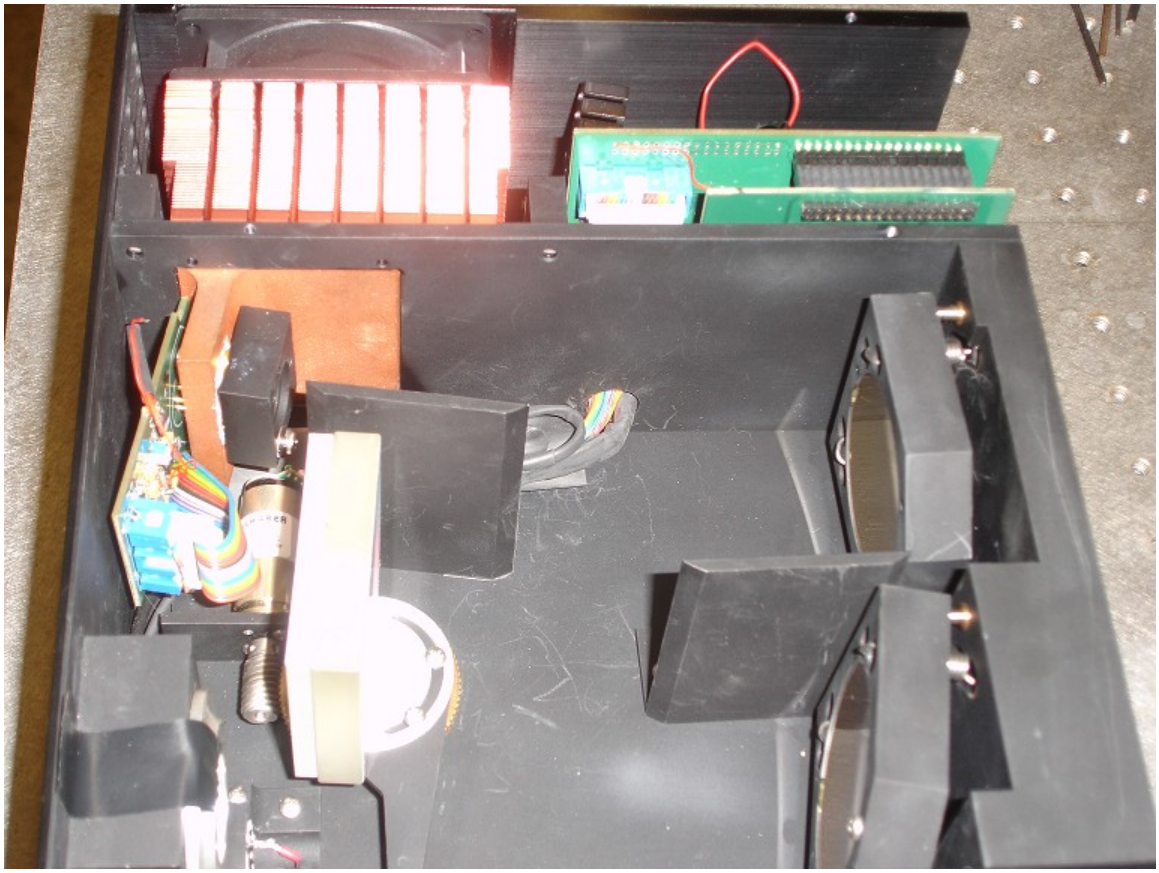

Fig. 14

were inscribed with a femtosecond Ti:sapphire laser by personnel at the Communications Research Center in Canada.

In Phase I of this project, the basic feasibility of this concept was demonstrated. A single-frequency diode laser was used as the source and the expected change in reflectivity was observed over a pressure range of about 3 atm. However, the error limits on the data were very large, which resulted from the fact that the reflectivity did not vary smoothly with the wavelength due to the highly multimoded nature of the sapphire fiber. It was therefore proposed that a broad band light source be used in Phase II, so that one can measure the shape of the entire reflected signal. By curve fitting, then, one should be able to determine the "peak" wavelength of the reflection. It was hoped that this procedure would lead to an acceptable uncertainty in the measurement.

Our first Phase II task was to determine the elastic limit of the sapphire FBG. To that end, a variable tension was applied to a 125 μm sapphire fiber containing a Bragg grating which was repeatedly heated to 300 ˚C and allowed to cool to ambient. Then the tension was released. It was found that the grating recovered to its original state up to a force of 9.9 N. On the next increment the fiber broke at the position of the grating. This result was reproduced for a second sapphire FBG prepared in an identical manner. One can infer from this that the rupture strain for the FBG is almost a factor of 4 lower than that for unradiated sapphire.

Given the low rupture strain of the sapphire FBG, in order to accommodate the minimum target range of 1 – 10 atm, the following parameters were selected for the pressure sensor: a sapphire fiber of 150 μm diameter so as to have a 40 % safety factor and a bellows with an effective area of 14 mm^2 and a spring rate of 30 N/mm. In the

meantime, a procedure for sealing the FBG inside the bellows was developed. A pin was used in this technique to keep the fiber from slipping through the end plate under even the maximum tension of 10 N. The sealing was then accomplished with the use of a high temperature elastomer. Following this procedure, two identical pressure sensors were fabricated.

To characterize the pressure sensor, light from a high power 940 nm LED was launched into one of the fibers on the bifurcated end of a 2 x 1 fiber coupler. The single-fiber end was then connected to the pressure sensor. The second fiber on the bifurcated end was connected to a fiber optic spectrometer. An example of the signal recorded by the spectrometer is shown in Fig. 15. In this figure the broad peak is due to reflections and scattering from the ends of the fibers and corresponds to the emission spectrum of the LED, while the narrow peak is produced by reflection caused by the sapphire FBG. To extract the reflected signal from the FBG alone, a separate spectrum of the LED was recorded and scaled to have the same value as the broad peak at the maximum. The latter was then subtracted from the combined reflected spectrum shown in Fig. 15 to yield the contribution from the FBG. The result is shown in Fig. 16.

The shoulders of the FBG reflection signal are shown on an expanded scale in Fig. 17. They were fitted to straight lines, and where the extensions of the latter intersect was taken to correspond to the maximum of the reflection peak. When a number of measurements were taken, an acceptable standard deviation was found. However, when the sapphire fiber was disconnected and then reconnected, the peak wavelength shifted by nearly 2 nm, which is as much as the expected shift for the entire 10 atm range. This was attributed to the highly multi-moded nature of the sapphire fiber. The distribution of

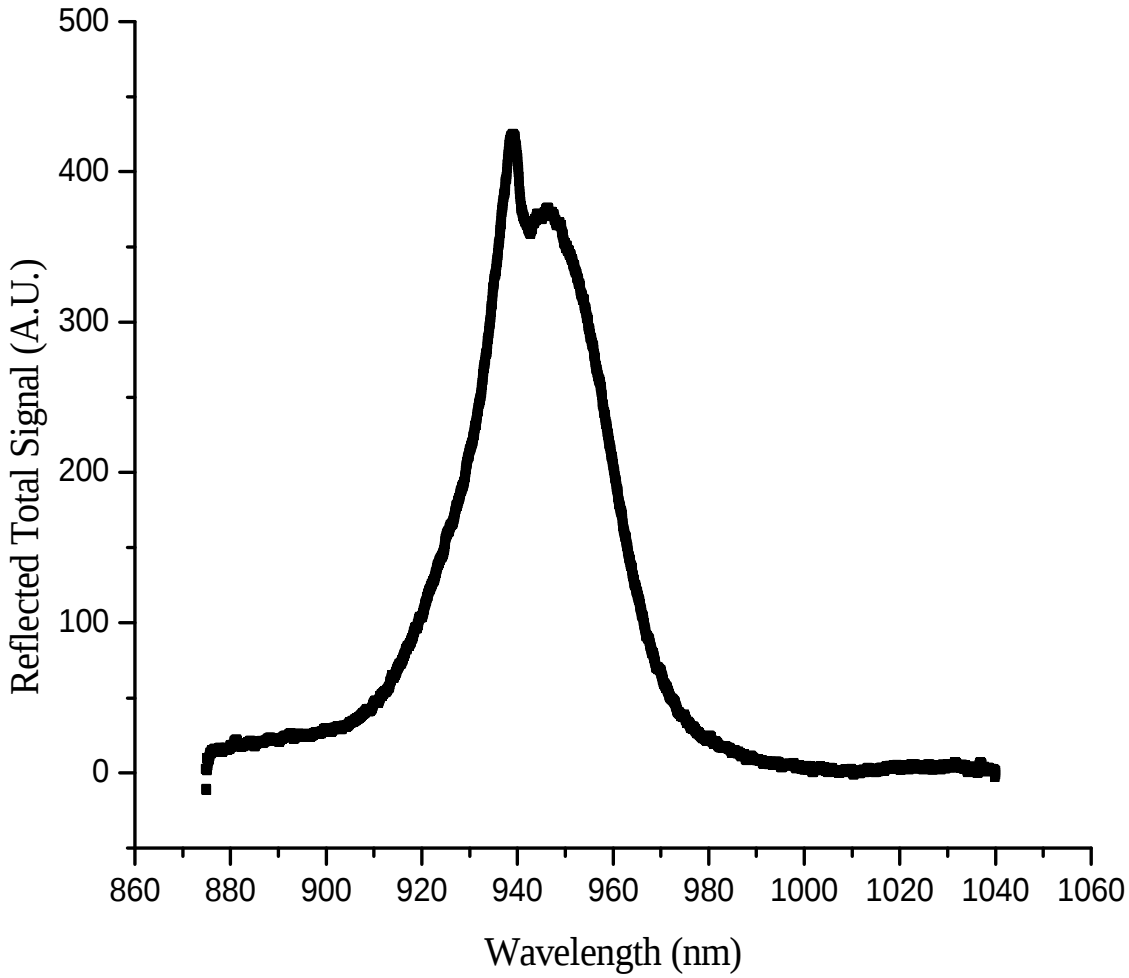
500
400
300
200
100
0
Reflected Total Signal (A.U.)
860
880
900
920
940
960
980
1000
1020
1040
1060
Wavelength (nm)

Fig. 15

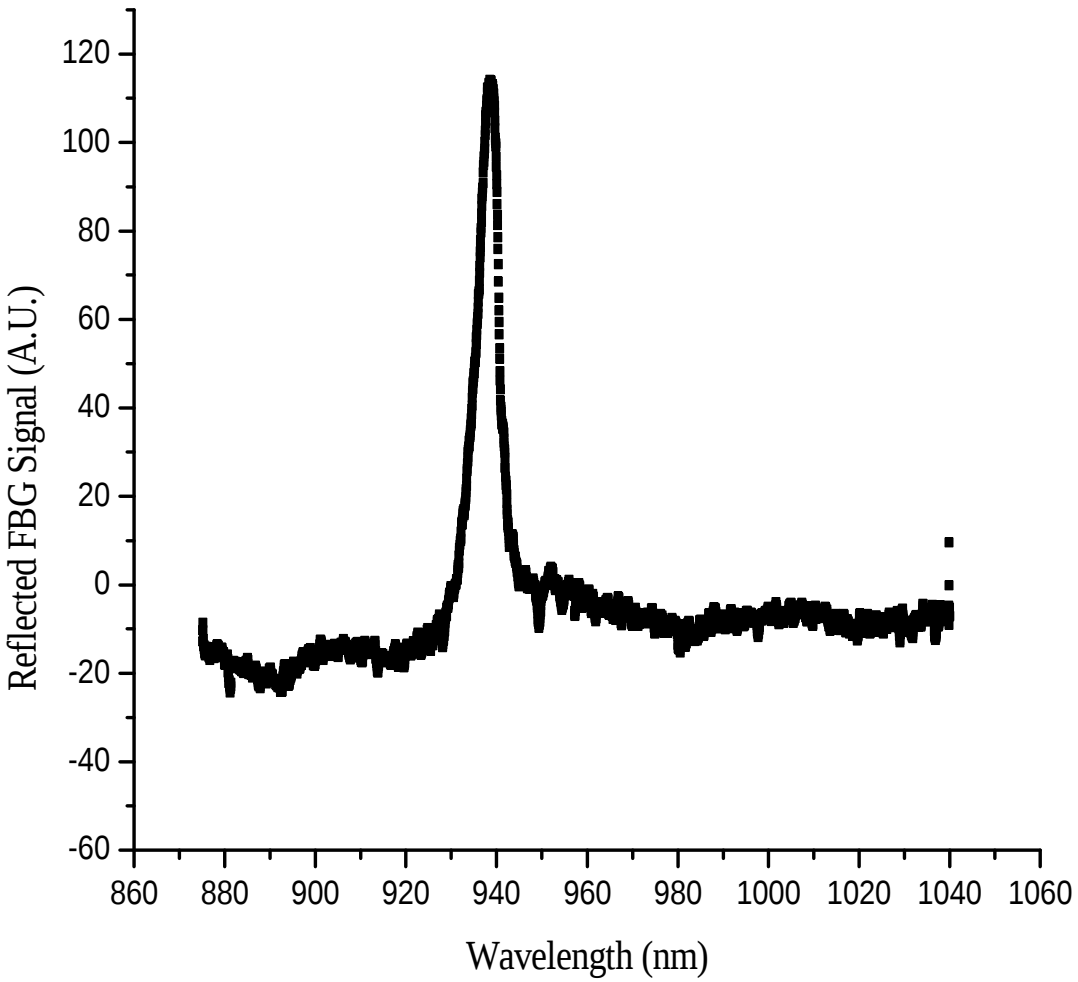
Reflected FBG Signal (A.U.)
120
100
80
60
40
20
0
-20
-40
-60
860
880
900
920
940
960
980
1000
1020
1040
1060
Wavelength (nm)

Fig. 16

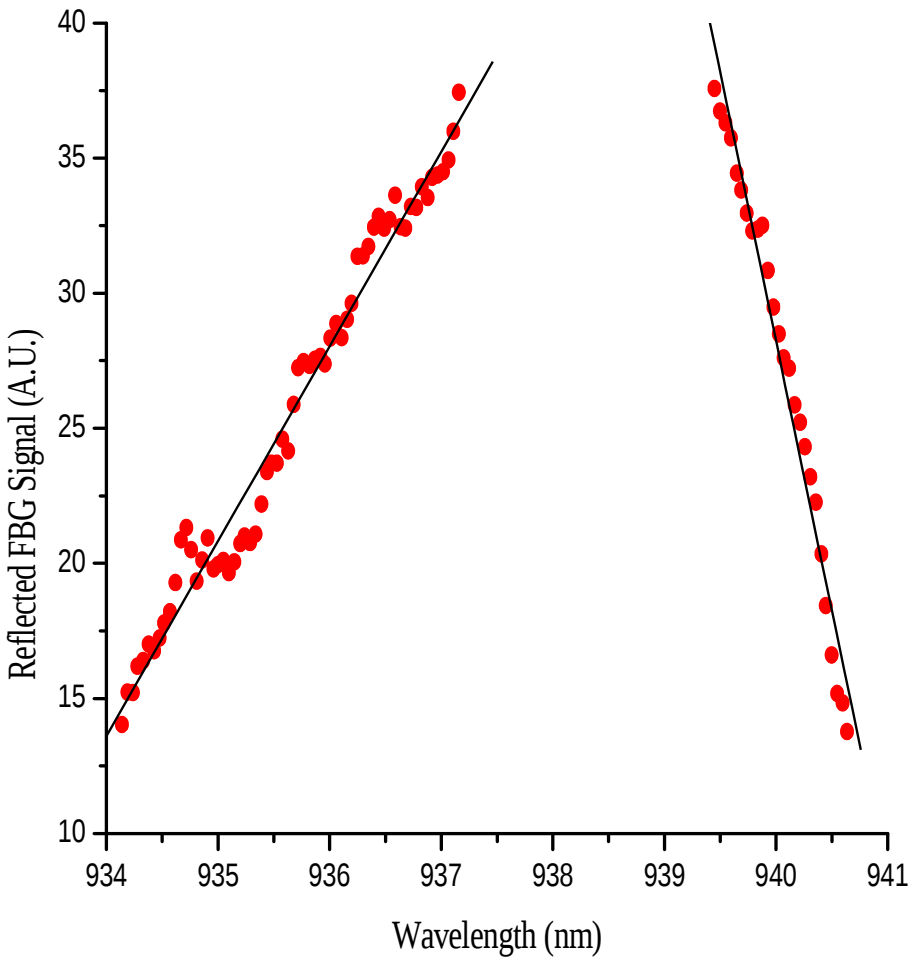
40
35
30
25
20
15
10
Reflected FBG Signal (A.U.)
934
935
936
937
938
939
940
941
Wavelength (nm)

Fig. 17

modes may depend sensitively on launch condition as well as any slight bend of the FBG. Efforts were made to excite as few modes as possible, consistent with retaining an adequate signal-to-noise level, by reducing the angular spread of the launch beam. These measures reduced the dependence of the peak wavelength on coupling condition to just under 1 nm.

Nevertheless, two pressure sensors were fabricated in the hope that, once the FBG is under tension, the coupling sensitivity would be further reduced. The finished pressure sensors were noticeably bent. To correct for the deformation, the bellows were placed in close-fitting tubes. It was found, however, that the fit could not be too tight if the bellows were to slide freely within the tube. As a result, the bend in the bellows could only be partially corrected.

The sensitivity of peak reflection wavelength to coupling condition was studied with one of the pressure sensors. After the sapphire FBG was connected to the 2 x 1 coupler, four successive measurements were made. Then the connector was rotated in ¼ turn increments, with four measurements taken at each azimuthal position. The results are shown in Table 1. It is seen that while the deviations at any one coupling position were acceptable, from one position to another the difference remained almost 1 nm. In other words, even with the FBG stretched taut, the sensitivity to coupling condition remained excessively large.

The second pressure sensor was placed in a pressure cell, and the peak FBG reflection wavelength was determined as the pressure was increased in three sequences and decreased in a fourth sequence. The data are shown in Table 2. Two trends are worth noting. Firstly, even with no change in coupling condition, the maximum

TABLE 1

FBG COUPLING TEST

Trial #	0 Turn (nm)	1/4 Turn (nm)	1/2 Turn (nm)	3/4 Turn (nm)
1	938.9849	938.6810	938.1170	938.2963
2	938.9480	938.6520	938.0599	938.1822
3	938.9593	938.6158	938.0269	938.1561
4	938.9914	938.5720	938.0998	938.2103
AVERAGE	938.9709	938.6302	938.0759	938.2112
ST. DEV.	0.0206	0.0471	0.0405	0.0609

TABLE 2

PRESSURE (atm)	UP TRIAL #1	UP TRIAL #2	UP TRIAL #3	DOWN TRIAL	Avg. (nm)	St. Dev. (nm)
1	940.3680	940.5333	940.5149	940.3496	940.4414	0.0960
2.4	940.3065	940.4019	940.4967	940.2220	940.3568	0.1187
3.7	940.2614	940.2316	940.2473	940.2099	940.2375	0.0221
5.1	940.2982	940.4838	940.4968	940.1687	940.3619	0.1575
6.4	940.1904	940.2104	940.2201	940.1732	940.1985	0.0210
7.8	940.2283	940.3669	940.3729	940.3088	940.3192	0.0672
9.2	940.2192	940.2300	940.2080	940.2356	940.2232	0.0122
10.5	940.4071	940.3941	940.3434	940.1178	940.3156	0.1347
11.7	940.2259	940.2020	940.1910	940.3596	940.2446	0.0780

reflection wavelength showed substantially more scatter at ambient pressure after each cycling than seen earlier for successive measurements with no change in pressure. Of much greater concern is the observed dependence of the peak wavelength on pressure. If there had not been any distortion of the bellows, the peak wavelength should have decreased by approximately 0.2 nm for each pressure increment. Instead, we saw a decrease of approximately 0.1 nm on the first two pressure increments and no discernable pattern thereafter. Our interpretation of these results is that initially the sensor's response was diminished because of friction between the bellows and the straightening tube into which it was inserted. At higher pressures, the bellows was further distorted and the friction increased. At the same time, the distortion altered the microbend in the fiber produced by the lack of perpendicularity between the endcap and the fiber. These effects combined to give an essentially unpredictable response of the sensor.

The strong sensitivity of the sapphire FBG to launch condition was unforeseen. Combined with the low rupture strain for the FBG, this effect implies a measurement uncertainty of approximately 25 % of the full range, which is clearly unacceptable. Also not expected was the strong frictional force between the bellows and the straightening tube, which makes reliable pressure measurement all but impossible. Together, these two deleterious effects make this particular pressure sensing concept a very unappealing one.

INTEGRATED SENSOR

An integrated probe consisting of a 65 μm sapphire fiber with the ends tapered up to 160 μm was fabricated. One of the large ends contained a section doped with Cr^{3+} for

temperature sensing. The 65 μm part was wound around a threaded cylinder with 1 cm radius to give a coil with 4.5 loops. The end view and side view of the assembled probe are shown in Fig. 18 and Fig. 19. Fig. 20 shows the probe in its test housing. The response of the temperature and chemical sensing elements were tested at room temperature first. For chemical sensing the 2.3 μm band in dodecane was used. Both behaved as expected. Unfortunately, during a dry run up to 300 ˚C the fiber broke. It is suspected that maybe the fiber was wound too tightly around the cylinder. At this time, work is continuing as part of MMI's IR & D program to better understand the failure of the coiled sapphire fiber at high temperatures.

PRODUCTS DEVELOPED

Before embarking on a full-scale commercialization effort of the dual temperature/chemical sensing system, we will start with the productization of the various components developed under this program. They include the monolithic sapphire/ruby fiber optic temperature sensor, the sapphire fiber evanescent field chemical sensor, the laser-driven fiber optic light source, and the fiber optic near/mid-IR spectrometer.

The monolithic construction of the sapphire/ruby temperature sensor makes it an exceptionally robust device both mechanically and chemically. Compared to other fiber optic temperature sensors on the market, it also has significantly higher maximum operating temperature. These features will allow it to not only successfully compete with currently available systems, but also find market niches such as process control in the rapidly expanding arena of microwave/RF powered manufacturing.

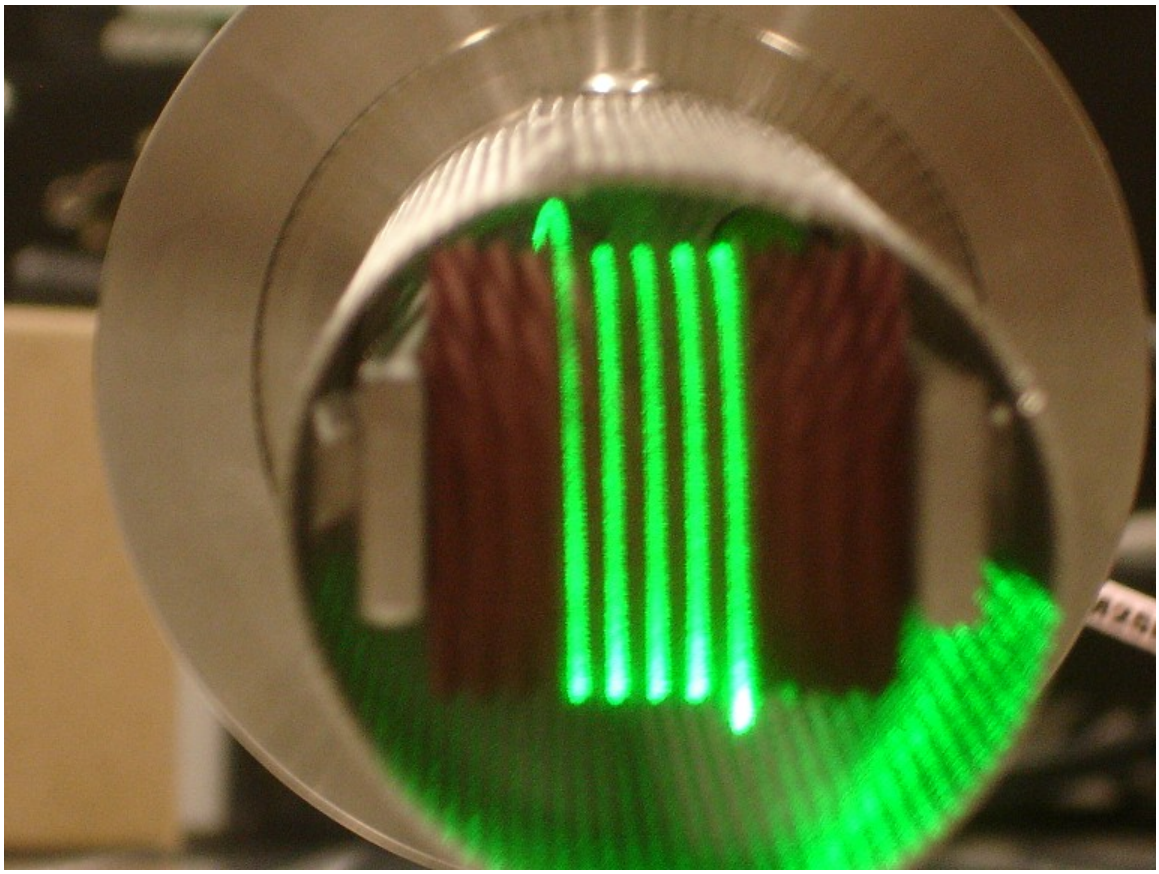

Fig. 18

Fig. 19

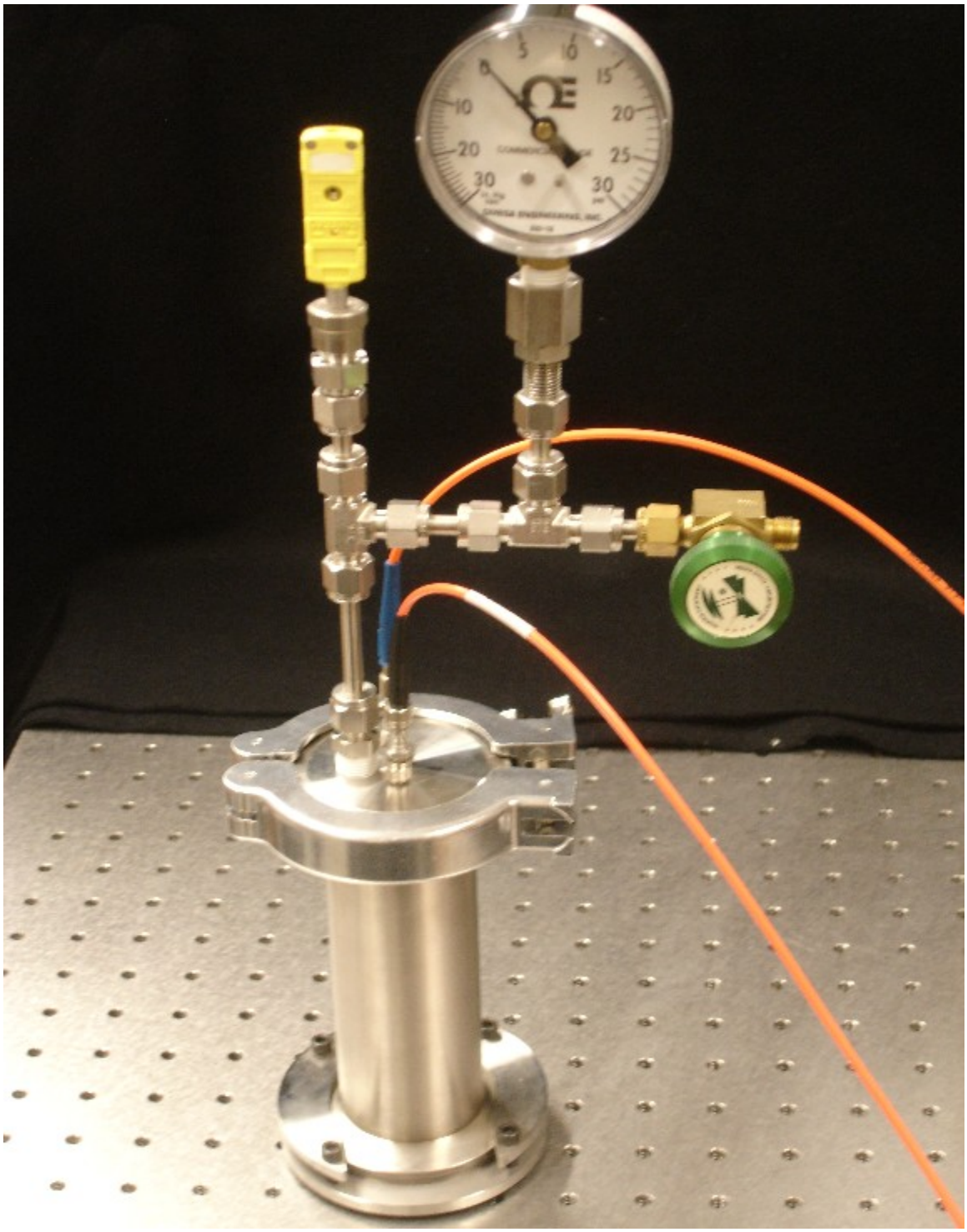

Fig. 20

The sapphire fiber evanescent field chemical sensor offers a totally new capability. By adjusting the depth of immersion of the coiled fiber, one can vary the interaction length by as much as two orders of magnitude. This means one can do both near-IR and mid-IR spectroscopy with a single probe. This novel capability will make the identification of chemicals both easier and faster, and should be an attractive feature for many researchers.

The near/mid-IR fiber optic spectrometer is intended to complement the evanescent-field chemical sensor. In addition to its spectral versatility, together with the evanescent-field sensor they offer a low-cost alternative to FTIR for process control. The scan-and-dwell feature of the spectrometer allows the system to measure absorption at a predetermined number of wavelengths with high speed. The quantification of this capability will be a primary Phase III task.

Likewise, the laser-driven fiber optic light source brings new perspective to IR spectroscopy. Our approach of fabricating the emitter makes it possible to customize the emission spectrum for specific applications. It is expected that a commercial unit with 2 – 3 interchangeable emitters will be available within the coming year. Additional emitters will be introduced with time after further R & D and according to customer interest.